MATHEMATICAL ENGINEERING
TECHNICAL REPORTS

An Energy-Conserving Galerkin Scheme for a Class of Nonlinear Dispersive Equations

Takayasu MATSUO and Hisashi YAMAGUCHI

METR 2008–14 March 2008

DEPARTMENT OF MATHEMATICAL INFORMATICS
GRADUATE SCHOOL OF INFORMATION SCIENCE AND TECHNOLOGY
THE UNIVERSITY OF TOKYO
BUNKYO-KU, TOKYO 113-8656, JAPAN

WWW page: http://www.i.u-tokyo.ac.jp/mi/mi-e.htm

An Energy-Conserving Galerkin Scheme for a Class of Nonlinear Dispersive Equations

Takayasu Matsuo
Department of Mathematical Informatics
Graduate School of Information Science and Technology
The University of Tokyo
matsuo@mist.i.u-tokyo.ac.jp

Hisashi Yamaguchi
Chuo Mitsui Asset Trust and Banking Company, Ltd.

March, 2008

Abstract

A Galerkin scheme is presented for a class of conservative nonlinear dispersive equations, such as the Camassa–Holm equation and the regularized long wave equation. The scheme has two advantageous features: first, it is conservative in that it keeps the discrete analogue of the continuous energy conservation property in the original equations; second, it can be formulated only with cheap H^1-elements even if the original equations include third derivative u_{xxx}. Numerical experiments confirm the stability and effectiveness of the proposed scheme.

1 Introduction

In this paper numerical integration of a class of nonlinear dispersive equations:

$$u_t - u_{xxt} + \kappa u_x + 3uu_x = \gamma(2u_x u_{xx} + uu_{xxx}), \qquad x \in \mathbb{R},\ t > 0, \tag{1}$$

is considered. The equation (1) describes a wide variety of nonlinear dispersive phenomena depending on the values of κ and γ. With $\kappa \geq 0, \gamma = 1$, it

reduces to the Camassa–Holm equation (CH):

$$u_t - u_{xxt} + \kappa u_x = 2u_x u_{xx} + u u_{xxx} - 3u u_x, \tag{2}$$

which models unidirectional propagation of shallow water waves [5, 6], with u representing the fluid velocity in the x direction (or equivalently the height of the fluid's free surface), and κ the critical shallow water wave speed. The CH has a bi-Hamiltonian structure, is completely integrable [17], and has global solutions [9]. It also has solitary waves, but they are in sharp contrast to, for example, those of the Korteweg–de Vries equation, in that the solitary waves become peaked in the limit of $\kappa \to 0$ (called "peakons"), which describe in physical context "wave-breaking" [27]. When $\kappa = 0, \gamma \in \mathbb{R}$, the equation reduces to the Dai equation [13]:

$$u_t - u_{xxt} + 3u u_x = \gamma(2u_x u_{xx} + u u_{xxx}), \tag{3}$$

which describes propagation of finite-length and small-amplitude waves in cylindrical compressible hyperelastic rods. In this case u represents the radial stretch, and γ the material constant which, for example, ranges from -29.4760 to 3.4174 [14]. Although this equation looks quite similar to the CH, its solutions behave in completely different manners depending on γ [11, 14]. For $\gamma < 1$, solitary waves of the Dai equation are smooth. When $\gamma = 1$ the equation reduces to the CH equation with $\kappa = 0$, and thus solitary waves become peaked. If γ exceeds one, the singularities in the solutions become even stronger such that at some points derivatives are no longer bounded ("cusped"); physically, it expresses the "rod-breaking." Another example of (1) is the so-called regularized long wave (or simply the BBM) equation [2]:

$$u_t - u_{xxt} = -3u u_x - u_x, \tag{4}$$

which is obtained by setting $\kappa = 1, \gamma = 0$. In contrast to the preceding two equations, all solutions of the BBM are global, and solitary waves are smooth.

Motivated by the physical and mathematical relevance of these PDEs, some effort have been already devoted to the numerical computation of the equation (1). Below are such examples. For the CH, several standard pseudospectral schemes [5, 6, 22], a finite-difference scheme [20], a specialized scheme using the multi-peakon structure of the equation [21], and a multi-symplectic scheme [8] have been studied. For the BBM, we refer the readers to [15, 19] and the references therein. For the Dai equation, we could not find any, which might be attributed to the fact that the equation itself is quite new (proposed in 1998).

The aim of the present paper is to give a new reliable numerical scheme for the equation (1), from a different perspective from the above mentioned numerical studies. The key fact here is that the equation (1) has an invariant under appropriate boundary conditions. With numerical analysis in mind, let us choose the periodic boundary condition:

$$u(x,t) = u(x+L,t), \qquad x \in (-\infty,\infty), t > 0. \tag{5}$$

Then we see the quantity

$$-\frac{1}{2}\int_0^L \left(\kappa u^2 + u^3 + \gamma u {u_x}^2\right) \mathrm{d}x \tag{6}$$

is strictly preserved along the solution (see Theorem 2.1). It often corresponds to some physical energies of fluids or rods, and thus is called the "energy." In the present paper, in the purpose of constructing a "reliable" numerical scheme, we demand our numerical scheme to keep this energy conservation property in discrete setting. In recent years, such "energy-conserving" numerical schemes have drawn much interest and been extensively studied for various PDEs, since they are more likely to give stabler and qualitatively better computations [3, 18, 25] (see also [23] for nearly-conservative method for Hamiltonian PDEs). To the best of the authors' knowledge, however, so far strictly conserving scheme for (1) has not yet been proposed in the literature (except an unpublished study on strictly conservative finite difference schemes for the CH [26], and a study on a nearly-conservative multi-symplectic scheme for the CH [8]). Our main idea for constructing a strictly-conservative scheme is to utilize the concept of "discrete partial derivatives," which has been introduced in [24] by one of the present authors for designing conservative (or dissipative, respectively) Galerkin schemes for certain conservative (dissipative) PDEs in variational form. It will be shown that with some trick the equation (1) can be also written in variational form, and the idea and tools above can be utilized for (1).

In this mission, we further like to demand that our numerical scheme is able to be formulated within the space H^1, the standard first-order Sobolev space, due to the following two reasons. First, simply from the computational perspective, we hope to keep the possibility of utilizing cheap H^1-elements (instead of relatively expensive C^1-elements). Second and more importantly, since the solutions of the target equation (1) can develop derivative singularities (e.g. peakons), it seems natural to work within the space H^1 rather than H^3 which is seemingly required to treat the third-order equation (1). This point seems to have not been explicitly emphasized in the existing numerical studies, where more or less stronger regularity is implicitly assumed by using some standard finite-difference or pseudospectral discretization.

With such a goal fixed—an energy-conserving scheme implementable within H^1—we face a big difficulty: as far as the authors know, there has been no H^1-formulation of the equation (1) in the literature that directly gives rise to the energy conservation property. Although some H^1-formulation have been found so far in order to justify peakons (see Section 2), the energy conservation property of their H^1 solutions can be proved only in so indirect manners that they can not be followed in discrete setting. As a solution to this issue, in this paper we present a new H^1-formulation of the problem from which the energy conservation property can be quite easily and directly derived.

The rest of the present paper is organized as follows. In Section 2, mathematical preliminaries regarding the target equation (1) are summarized. Then in Section 3, the proposed scheme is presented, and its properties are discussed. Its application examples are shown in Section 4 with various numerical experiments that illustrate the effectiveness of the proposed scheme.

2 Properties of the target equation

Some mathematical properties of the target equation (1) are summarized. Let us denote by $\mathbb{S}$ the torus of length L, and consider that the target equation is defined on it. We denote by $L^2(\mathbb{S})$ the standard L^2 space over $\mathbb{S}$, and by $(f,g) = \int_0^L fg\,\mathrm{d}x$ its associated norm. We also denote by $H^n(\mathbb{S})$ the standard Sobolev space over $\mathbb{S}$.

The equation (1) can be viewed as a gradient flow:

$$\left(1 - \frac{\partial^2}{\partial x^2}\right) u_t = \left(\frac{\delta G}{\delta u}\right)_x, \tag{7}$$

where

$$G(u, u_x) = -\frac{\kappa u^2 + u^3 + \gamma u {u_x}^2}{2}. \tag{8}$$

The symbol

$$\frac{\delta G}{\delta u} = \frac{\partial G}{\partial u} - \frac{\partial}{\partial x}\frac{\partial G}{\partial u_x} \tag{9}$$

denotes the standard variational derivative of $G(u, u_x)$ with respect to u. If we further introduce an operator $\mathcal{K} = (1 - \partial^2/\partial x^2)^{-1}$, which is a map $L^2(\mathbb{S}) \to H^2(\mathbb{S})$ [4], the equation can be rewritten as

$$u_t = \mathcal{K}\left(\frac{\delta G}{\delta u}\right)_x. \tag{10}$$

With the Green function:

$$k(x) = \frac{\cosh(x - L[x/L] + L/2)}{2\sinh(L/2)}, \tag{11}$$

the operator $\mathcal{K}$ can be expressed in terms of the convolution

$$(\mathcal{K}f)(x) = (k * f)(x) = \int_0^L k(x-\xi)f(\xi)\mathrm{d}\xi. \tag{12}$$

The conservation property (6) is summarized in the following theorem, which holds for general $G(u, u_x)$ (i.e. not only for the one defined in (8) but also for other functions). Observe that the variational derivative plays a central role in the proof, and the concrete form of G is not relevant here.

Theorem 2.1 (Conservation property of (1)). *Suppose $u(\cdot,t) \in H^3(\mathbb{S}), u_t(\cdot,t) \in H^1(\mathbb{S})$, and $G(u,u_x)$ is sufficiently smooth with respect to its arguments. Then,*

$$\frac{\mathrm{d}}{\mathrm{d}t}\int_0^L G\,\mathrm{d}x = 0. \tag{13}$$

Proof.

$$\begin{aligned}\frac{\mathrm{d}}{\mathrm{d}t}\int_0^L G\,\mathrm{d}x &= \int_0^L \left(\frac{\partial G}{\partial u}u_t + \frac{\partial G}{\partial u_x}u_{tx}\right)\mathrm{d}x = \int_0^L \frac{\delta G}{\delta u}u_t\,\mathrm{d}x + \left[\frac{\partial G}{\partial u_x}u_t\right]_0^L \\ &= \int_0^L \frac{\delta G}{\delta u}\mathcal{K}\left(\frac{\delta G}{\delta u}\right)_x \mathrm{d}x = 0.\end{aligned}$$

In the third equality, the boundary term is dropped due to the periodicity. In the last equality, an identity $(\mathcal{K}f_x, f) = 0$ which holds for any $f \in H^1(\mathbb{S})$ is used. □

The story above makes sense only when $u(\cdot,t) \in H^3(\mathbb{S})$ since $(\delta G/\delta u)_x$ essentially includes u_{xxx}. However, in order to allow singular solutions like peakons, an $H^1(\mathbb{S})$-formulation is inevitably required. In the critical CH ($\kappa = 0$) case, such a form is given in [9] (see also [12]):

$$u_t + \frac{1}{2}\left(u^2 + \mathcal{K}\left(u^2 + \frac{{u_x}^2}{2}\right)\right)_x = 0, \tag{14}$$

which makes sense for $u(\cdot,t) \in H^1(\mathbb{S})$. In the present paper, however, we do not adopt this expression, since it seems that the conservation property of (14) can not be directly established, and thus (14) is not a convenient in our project. Actually, in [10], the conservation property of (14) is established

by expressing the target H^1-solution of (14) as the limit of a series of energy-conserving H^3-solutions of (2) (with $\kappa = 0$). It seems difficult to do a similar thing in discrete setting.

Instead we propose to employ the following set of weak forms. Recalling the relation (9), we rewrite the equation (10) to the problem: Find $u(\cdot,t), p(\cdot,t) \in H^1(\mathbb{S})$ such that for any $v_1, v_2 \in H^1(\mathbb{S})$,

$$(u_t, v_1) = (\mathcal{K} p_x, v_1), \tag{15}$$

$$(p, v_2) = \left(\frac{\partial G}{\partial u}, v_2\right) + \left(\frac{\partial G}{\partial u_x}, (v_2)_x\right). \tag{16}$$

It is obvious that the solution $u(\cdot,t) \in H^3(\mathbb{S})$ that solves (10) also solves this set of weak forms by setting $p = \delta G/\delta u$. From the weak forms (15), (16) , the desired conservation property can be successfully deduced as shown in the next theorem. The deduction can be done completely in an abstract way as in Theorem 2.1; in this case, however, the key tool is the *partial* derivatives $\partial G/\partial u, \partial G/\partial u_x$, instead of the *variational* derivative $\delta G/\delta u$.

Theorem 2.2 (Conservation property of the weak forms (15), (16))**.** *Suppose $u(\cdot,t), p(\cdot,t) \in H^1(\mathbb{S})$ are the solution of the weak forms* (15) *and* (16)*. Also assume that G is sufficiently smooth and $u_t(\cdot,t) \in H^1(\mathbb{S})$. Then it holds*

$$\frac{\mathrm{d}}{\mathrm{d}t} \int_0^L G \,\mathrm{d}x = 0. \tag{17}$$

Proof.

$$\frac{\mathrm{d}}{\mathrm{d}t} \int_0^L G \,\mathrm{d}x = \left(\frac{\partial G}{\partial u}, u_t\right) + \left(\frac{\partial G}{\partial u_x}, u_{tx}\right) = (p, u_t) = (\mathcal{K} p_x, p) = 0. \tag{18}$$

The first equality is just the chain rule. The second equality follows from (16) with $v_2 = u_t$, and the third one from (15) with $v_1 = p$. □

Remark 2.1. From the mathematical point of view, it should be asked if and under what conditions the system of the weak forms (15), (16) has a solution in $H^1(\mathbb{S})$ (as noted above, when (10) has a $H^3(\mathbb{S})$ solution, it also solves the system; in this case, only its uniqueness matters). In the present paper, however, we like to leave this open, since the situation drastically varies depending on the concrete form of $G(u, u_x)$ (or equivalently, the parameters κ, γ in the equation (1)), and the question itself seems to be a big mathematical challenge which has not yet been completely solved even in the case of the original PDE (1). Interested readers may refer [7] which discusses the local well-posedness of (1). ■

3 Galerkin scheme and its properties

An energy-preserving scheme is constructed and its properties are shown. As seen in the previous section, the partial derivatives $\partial G/\partial u, \partial G/\partial u_x$ play a central role in proving the conservation property (Theorem 2.2). This motivates us to employ the idea of the "discrete partial derivatives" [24] for constructing an energy-preserving Galerkin scheme. For readers' convenience, the idea is briefly summarized first.

Following [24], we here consider generalized energy functions of the form

$$G(u, u_x) = \sum_{l=1}^{M} f_l(u) g_l(u_x), \tag{19}$$

where $M \in \{1, 2, \ldots\}$, and f_l, g_l are sufficiently smooth real-valued functions. The target energy function (8) in this paper is a special case of (19), where $M = 3$, $f_1 = -\kappa u^2/2, g_1 = 1$, $f_2 = -u^3/2, g_2 = 1$, and $f_3 = -\gamma u/2, g_3 = {u_x}^2$.

Let us denote Galerkin approximate solutions by $u^{(m)} \simeq u(x, m\Delta t)$ (Δt is the time mesh size). Then "discrete partial derivatives" of the energy function (19) are defined as follows.

Definition 3.1 (Discrete partial derivatives [24]). *We call the discrete quantities*

$$\frac{\partial G_{\rm d}}{\partial (u^{(m+1)}, u^{(m)})} :\equiv \sum_{l=1}^{M} \left(\frac{f_l(u^{(m+1)}) - f_l(u^{(m)})}{u^{(m+1)} - u^{(m)}} \right) \left(\frac{g_l(u_x^{(m+1)}) + g_l(u_x^{(m)})}{2} \right) \tag{20}$$

$$\frac{\partial G_{\rm d}}{\partial (u_x^{(m+1)}, u_x^{(m)})} :\equiv \sum_{l=1}^{M} \left(\frac{f_l(u^{(m+1)}) + f_l(u^{(m)})}{2} \right) \left(\frac{g_l(u_x^{(m+1)}) - g_l(u_x^{(m)})}{u_x^{(m+1)} - u_x^{(m)}} \right) \tag{21}$$

the "discrete partial derivatives," which corresponds to $\partial G/\partial u$ and $\partial G/\partial u_x$, respectively[1].

For the function $G(u, u_x)$ defined in (8), the concrete forms of the discrete partial derivatives are

$$\begin{aligned} \frac{\partial G_{\rm d}}{\partial (u^{(m+1)}, u^{(m)})} &= -\kappa \left(\frac{u^{(m+1)} + u^{(m)}}{2} \right) - \frac{(u^{(m+1)})^2 + u^{(m+1)} u^{(m)} + (u^{(m)})^2}{2} \\ &\quad - \gamma \left(\frac{(u_x^{(m+1)})^2 + (u_x^{(m)})^2}{4} \right), \end{aligned} \tag{22}$$

$$\frac{\partial G_{\rm d}}{\partial (u_x^{(m+1)}, u_x^{(m)})} = -\gamma \left(\frac{u^{(m+1)} + u^{(m)}}{2} \right) \left(\frac{u_x^{(m+1)} + u_x^{(m)}}{2} \right). \tag{23}$$

[1] Expressions similar to $(f(a) - f(b))/(a - b)$ should be interpreted as $f'(a)$ when $a = b$.

It can be easily verified that, corresponding to the continuous chain rule:

$$\frac{\mathrm{d}}{\mathrm{d}t}\int_0^L G(u,u_x)\mathrm{d}x = \int_0^L \left(\frac{\partial G}{\partial u}u_t + \frac{\partial G}{\partial u_x}u_{xt}\right)\mathrm{d}x,$$

the following discrete chain rule holds (hereafter $G(u^{(m)}, u_x^{(m)})$ is abbreviated as $G(u^{(m)})$ to save space.)

Theorem 3.1 (Discrete chain rule [24]). *Concerning the discrete partial derivatives* (20) *and* (21)*, the following identity holds.*

$$\begin{aligned}\frac{1}{\Delta t}\int_0^L \left(G(u^{(m+1)}) - G(u^{(m)})\right)\mathrm{d}x &= \int_0^L \left\{\frac{\partial G_\mathrm{d}}{\partial(u^{(m+1)}, u^{(m)})}\left(\frac{u^{(m+1)} - u^{(m)}}{\Delta t}\right)\right. \\ &\left. + \frac{\partial G_\mathrm{d}}{\partial(u_x^{(m+1)}, u_x^{(m)})}\left(\frac{u_x^{(m+1)} - u_x^{(m)}}{\Delta t}\right)\right\}\mathrm{d}x. \qquad (24)\end{aligned}$$

With these discrete partial derivatives, we define an abstract scheme for the weak forms (15) and (16) as follows. Let $S_1, S_2 \in H^1(\mathbb{S})$ be appropriately chosen trial spaces, and $W_1, W_2 \in H^1(\mathbb{S})$ test spaces. In the subsequent application examples, they shall be chosen to the standard periodic piecewise linear function space (the so-called "P1-elements"); for the moment, however, we would rather like to leave them open in order to keep the flexibility of the scheme.

Scheme 3.1 (Abstract Galerkin scheme for (15),(16)). *Suppose that* $u^{(0)}(x)$ *is given in* S_2*. Find* $u^{(m+1)} \in S_2$, $p^{(m+\frac{1}{2})} \in S_1$ $(m = 0, 1, 2, \ldots)$ *such that, for any* $v_1 \in W_1$ *and* $v_2 \in W_2$*,*

$$\begin{aligned}\left(\frac{u^{(m+1)} - u^{(m)}}{\Delta t}, v_1\right) &= \left(\mathcal{K}(p^{(m+\frac{1}{2})})_x, v_1\right), \qquad (25)\\ \left(p^{(m+\frac{1}{2})}, v_2\right) &= \left(\frac{\partial G_\mathrm{d}}{\partial(u^{(m+1)}, u^{(m)})}, v_2\right) \\ &\quad + \left(\frac{\partial G_\mathrm{d}}{\partial(u_x^{(m+1)}, u_x^{(m)})}, (v_2)_x\right). \qquad (26)\end{aligned}$$

The scheme enjoys the next conservation property. The proof can be done analogously to the continuous case.

Theorem 3.2 (Conservation property of Scheme 3.1). *Assume the trial and test spaces* S_1, S_2, W_1 *and* W_2 *are set such that* (i) $(u^{(m+1)} - u^{(m)})/\Delta t \in W_2$ *;* *and* (ii) $S_1 \subseteq W_1$*. Then Scheme 3.1 is conservative in the sense that*

$$\frac{1}{\Delta t}\int_0^L \left(G(u^{(m+1)}) - G(u^{(m)})\right)\mathrm{d}x = 0, \qquad m = 0, 1, 2, \ldots.$$

Proof.

$$\begin{aligned}
&\frac{1}{\Delta t}\int_0^L \left(G(u^{(m+1)}) - G(u^{(m)})\right) \mathrm{d}x \\
&= \left(\frac{\partial G_{\mathrm{d}}}{\partial(u^{(m+1)}, u^{(m)})}, \frac{u^{(m+1)} - u^{(m)}}{\Delta t}\right) + \left(\frac{\partial G_{\mathrm{d}}}{\partial(u_x^{(m+1)}, u_x^{(m)})}, \frac{u_x^{(m+1)} - u_x^{(m)}}{\Delta t}\right) \\
&= \left(p^{(m+\frac{1}{2})}, \frac{u^{(m+1)} - u^{(m)}}{\Delta t}\right) \\
&= \left(\mathcal{K}(p^{(m+\frac{1}{2})})_x, p^{(m+\frac{1}{2})}\right) = 0.
\end{aligned}$$

The first equality follows from the discrete chain rule (Theorem 3.1). The second one is shown by using the equation (26) with $v_2 = (u^{(m+1)} - u^{(m)})/\Delta t$ (the substitution is allowed by the assumption (i)), while the third one is given by using the equation (25) with $v_1 = p^{(m+\frac{1}{2})}$ (allowed by the assumption (ii)). □

Under the periodic boundary condition (5), it is natural to take $S_1 = S_2 = W_1 = W_2$. For example, in the finite-element context, all of them can be chosen to the same P1, P2, or higher-order elements. It is also possible to employ finite-dimensional Fourier (or Chebyshev and so on) space, which results in the so-called Fourier (Chebyshev) Galerkin schemes. In any cases, the assumptions in Theorem 3.2 are automatically satisfied as far as $S_1 = S_2 = W_1 = W_2$, and the resulting schemes become conservative.

Note that Scheme 3.1 makes sense and Theorem 3.2 holds for *any* energy function $G(u, u_x)$ in the form (19). Thus, they cover not only the target equation (1) but also similar variants that can be written in the variational form (7).

Remark 3.1. The equation (10) can also be viewed as a conservation law:

$$u_t - \left(\mathcal{K}\frac{\delta G}{\delta u}\right)_x = 0, \tag{27}$$

(note that for $f \in H^1(\mathbb{S})$ it holds $(\mathcal{K}f)_x = \mathcal{K}(f_x)$), and there is another invariant:

$$\frac{\mathrm{d}}{\mathrm{d}t}\int_0^L u \,\mathrm{d}x = \left(\mathcal{K}\left(\frac{\delta G}{\delta u}\right)_x, 1\right) = 0. \tag{28}$$

The final equality follows from an identity $((\mathcal{K}f)_x, 1) = 0$ which holds for any $f \in H^1(\mathbb{S})$. Scheme 3.1 also conserves this invariant:

$$\frac{1}{\Delta t}\int_0^L \left(u^{(m+1)} - u^{(m)}\right) \mathrm{d}x = (\mathcal{K}(p^{(m+\frac{1}{2})})_x, 1) = 0, \quad m = 0, 1, 2, \ldots. \tag{29}$$

■

Remark 3.2. Mathematically, the guarantees of the existence, uniqueness, stability, and convergence of the solutions of Scheme 3.1 should be given. This issue is, however, closely connected to the solvability of the continuous problem (15) and (16), which is set outside the scope of this paper as mentioned in Remark 2.1 . Thus we also like to leave such mathematical studies of Scheme 3.1 (save for the strict conservation properties) as future works. Instead, below we give various numerical experiments which support the stability and effectiveness of the proposed scheme. ■

4 Application examples

Scheme 3.1 is tested for the three PDEs mentioned in the introduction.

4.1 Common settings of the experiments

The spatial period $[0, L]$ is divided into N grids (either equispaced or non-equispaced), whose mesh points are denoted by x_j $(j = 0, 1, \ldots, N)$ $(x_0 = 0, x_N = L)$. We then employ the standard periodic piecewise-linear function space $S_{\mathrm{p}} \subseteq H^1(\mathbb{S})$ over the mesh; i.e., we set $S_1 = S_2 = W_1 = W_2 = S_{\mathrm{p}}$ in Scheme 3.1. Given the approximation space, the concrete form of Scheme 3.1 is

$$A\left(\frac{\boldsymbol{u}^{(m+1)} - \boldsymbol{u}^{(m)}}{\Delta t}\right) = K\boldsymbol{p}^{(m+\frac{1}{2})}, \tag{30}$$

$$A\boldsymbol{p}^{(m+\frac{1}{2})} = \boldsymbol{f}(\boldsymbol{u}^{(m+1)}, \boldsymbol{u}^{(m)}), \tag{31}$$

where $\boldsymbol{u}^{(m)} = (u^{(m)}(x_0), \ldots, u^{(m)}(x_{N-1}))^{\mathrm{T}}$, $\boldsymbol{p}^{(m+\frac{1}{2})} = (p^{(m+\frac{1}{2})}(x_0), \ldots, p^{(m+\frac{1}{2})}(x_{N-1}))^{\mathrm{T}}$, and $\boldsymbol{f}(\boldsymbol{u}^{(m+1)}, \boldsymbol{u}^{(m)})$ is the vector arising from the right hand side of (26) which in general nonlinearly include $\boldsymbol{u}^{(m+1)}$ and $\boldsymbol{u}^{(m)}$. The matrix A is the standard mass matrix whose elements are $A_{ij} = (\phi_i, \phi_j)$, where ϕ_i $(i = 0, \ldots, N-1)$ are the standard basis functions of S_{p}, and $K_{ij} = (\mathcal{K}(\phi_i)_x, \phi_j)$. Note that the matrices A and K depend only on the approximate space (i.e. the mesh), and can be prepared in prior to the time evolution process. The preparation of the matrix K involves the computation of convolutions, which can be done by hand in the case of S_{p}. When more general approximate spaces are required, it is also possible to employ some numerical integrator with sufficient accuracy. Since the matrix A is invertible, the equations (30) and (31) immediately reduce to

$$A\left(\frac{\boldsymbol{u}^{(m+1)} - \boldsymbol{u}^{(m)}}{\Delta t}\right) = KA^{-1}\boldsymbol{f}(\boldsymbol{u}^{(m+1)}, \boldsymbol{u}^{(m)}). \tag{32}$$

That is, the computation of the intermediate variable $\boldsymbol{p}^{(m+\frac{1}{2})}$ can be skipped, and the dimension of the system to be solved is N, instead of $2N$. In what follows, our numerical calculations are based on this expression.

The nonlinear equations (32) should be solved by some iterative method. A convenient way is to use some reliable numerical Newton library. In the experiments below, the routine `imsl_d_zeros_sys_eqn` in the IMSL was used.

4.2 The limiting Camassa–Holm equation

Originally, the Camassa–Holm (CH) equation (2) only makes sense for $\kappa > 0$ in physical context, since κ corresponds to the critical shallow water speed that should be strictly positive (see [5]). Mathematically, however, main interest is usually on the limiting case $\kappa = 0$, where solitons become peaked. Below we consider this case. The concrete form of Scheme 3.1 then becomes as follows. With the function

$$G(u, u_x) = -\frac{u^3 + u{u_x}^2}{2}, \tag{33}$$

which is obtained by setting $\kappa = 0,\ \gamma = 1$ in (8), the discrete partial derivatives (22) and (23) become

$$\begin{aligned} \frac{\partial G_{\mathrm{d}}}{\partial(u^{(m+1)}, u^{(m)})} &= -\frac{(u^{(m+1)})^2 + u^{(m+1)}u^{(m)} + (u^{(m)})^2}{2} \\ &\quad - \left(\frac{(u_x^{(m+1)})^2 + (u_x^{(m)})^2}{4}\right), \end{aligned} \tag{34}$$

$$\frac{\partial G_{\mathrm{d}}}{\partial(u_x^{(m+1)}, u_x^{(m)})} = -\left(\frac{u^{(m+1)} + u^{(m)}}{2}\right)\left(\frac{u_x^{(m+1)} + u_x^{(m)}}{2}\right). \tag{35}$$

Note that for the energy function (33) the (continuous) partial derivatives are

$$\frac{\partial G}{\partial u} = -\frac{3}{2}u^2 - \frac{1}{2}{u_x}^2 \quad \text{and} \quad \frac{\partial G}{\partial u_x} = -uu_x,$$

and we can see the correspondence between the continuous and discrete ones. Substituting the discrete partial derivatives into Scheme 3.1, we obtain the concrete form of the scheme, which is then implemented as described in Section 4.1.

For comparison, the following two implicit schemes have been also tested;

The Crank–Nicolson scheme:

$$\left(\frac{u^{(m+1)}-u^{(m)}}{\Delta t}, v_1\right) = \left(\mathcal{K}(p^{(m+\frac{1}{2})})_x, v_1\right) \tag{36}$$

$$\begin{aligned}\left(p^{(m+\frac{1}{2})}, v_2\right) &= -\left(\frac{3}{2}\left(\frac{u^{(m+1)}+u^{(m)}}{2}\right)^2 + \frac{1}{2}\left(\frac{u_x^{(m+1)}+u_x^{(m)}}{2}\right)^2, v_2\right) \\ &\quad -\left(\left(\frac{u^{(m+1)}+u^{(m)}}{2}\right)\left(\frac{u_x^{(m+1)}+u_x^{(m)}}{2}\right), (v_2)_x\right),\end{aligned} \tag{37}$$

and the implicit Euler scheme:

$$\left(\frac{u^{(m+1)}-u^{(m)}}{\Delta t}, v_1\right) = \left(\mathcal{K}(p^{(m+\frac{1}{2})})_x, v_1\right) \tag{38}$$

$$\begin{aligned}\left(p^{(m+\frac{1}{2})}, v_2\right) &= -\left(\frac{3}{2}\left(u^{(m+1)}\right)^2 + \frac{1}{2}\left(u_x^{(m+1)}\right)^2, v_2\right) \\ &\quad -\left(u^{(m+1)}u_x^{(m+1)}, (v_2)_x\right).\end{aligned} \tag{39}$$

Note that, since all of these schemes are based on the same weak forms (15) and (16), the spatial discretization is exactly the same, and only the temporal discretizations are different.

First, the three schemes are tested on the equispaced mesh with $L = 40$ and $N = 200$ (thus $\Delta x = 0.2$). The initial data is $u(x,0) = 5e^{-|x-x_a|} + 2e^{-|x-x_b|}$, where $x_a = (200/3 + 1/2)\Delta x$ and $x_b = (400/3 + 1/2)\Delta x$. Since larger peakons are faster, the larger peakon initially centered at x_a overtakes the smaller one at x_b as time passes. Figure 1 shows the numerical results obtained by the three schemes. According to the figure, both the proposed conservative scheme and the Crank–Nicolson scheme seem to correctly track the overtaking phenomenon (note that since now the periodic boundary condition is applied, the outgoing peakons come back to the interval from the left boundary). On the other hand, in the implicit Euler case, although the computation itself is stable, the peakons gradually become flattened. Figure 2 shows the evolution of the energy $\int_0^L G(u^{(m)})\mathrm{d}x$; the left figure shows the evolution near the starting time, and the right figure the overall profile. As suggested in the wave pattern in Figure 1, we observe strong energy dissipation in the case of the implicit Euler scheme (see left figure); the energy rapidly tends to zero. Although in Figure 1 the results by the proposed conservative scheme and the Crank–Nicolson scheme look quite similar, the energy profiles are considerably different (see right figure). In the proposed conservative scheme, the energy is strictly conserved to the machine accuracy, while in the Crank–Nicolson scheme it drifts.

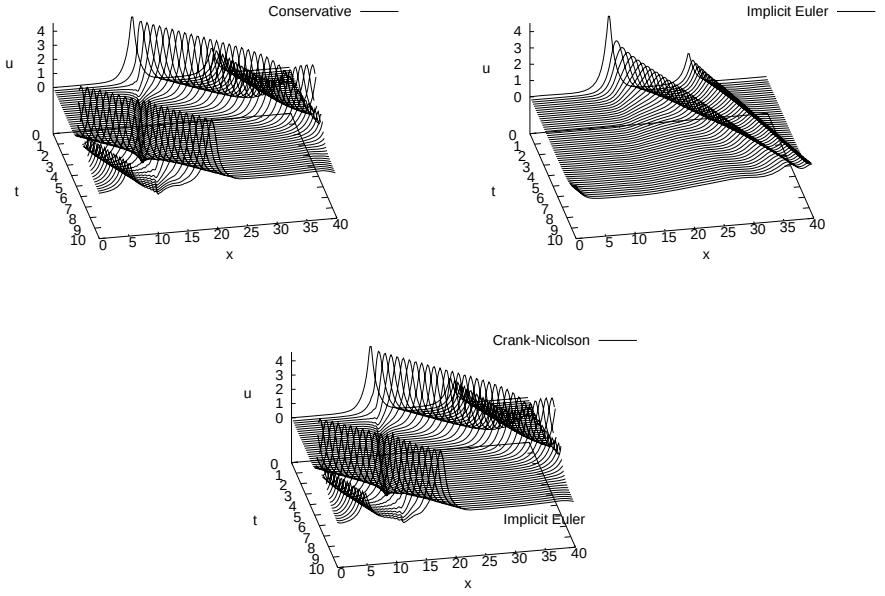

Figure 1: Evolution of the two peakons; (top-left) the conservative scheme, (top-right) the implicit Euler scheme, (bottom) the Crank–Nicolson scheme

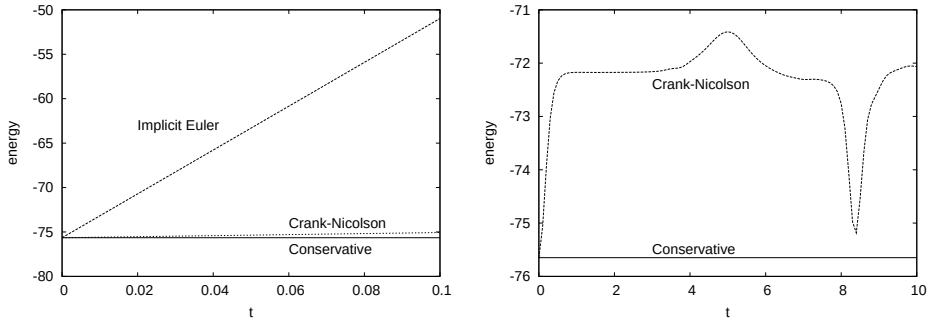

Figure 2: Evolution of the energies (two peakons case); (left) detailed profile around the origin, (right) global profile

Next, in order to check the long-time stability, the problem is solved for $0 \leq t \leq 70$ with the time mesh size $\Delta t = 0.02$ and the number of spatial grid points $N = 400$ ($\Delta x = 0.1$). With these parameters, the larger peakon goes round the spatial interval about ten times. The conservative scheme successfully integrates the problem with the energy strictly kept (Figure 3 (left) and Figure 4). In the Crank–Nicolson case, the energy is nearly conserved in the early stage $0 \leq t \leq 20$; the energy periodically oscillates and stays around the exact value. As time passes, however, the oscillation becomes irregular ($20 \leq t \leq 50$), and then completely unstable ($50 \leq t \leq 70$). This instability can be observed in the wave pattern in Figure 3, where the peakons in the Crank–Nicolson case are completely broken at $t = 70$. For $t \geq 70$, it turns out that the numerical Newton solver does not work in the Crank–Nicolson scheme, and it is impossible to continue the computation. This result strongly suggests that the conservative scheme is in fact more reliable than the standard Crank–Nicolson scheme.

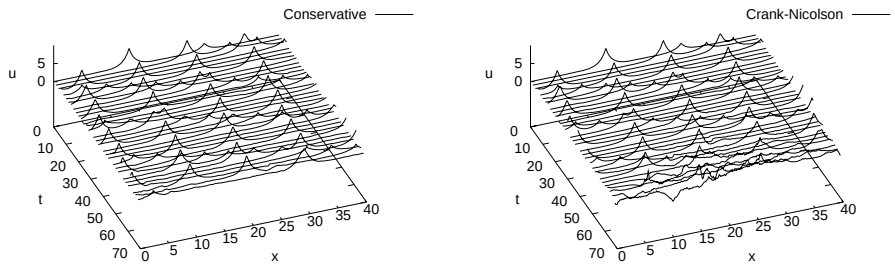

Figure 3: Long-time computation of the two-peakons problem; (left) the conservative scheme, (right) the Crank–Nicolson scheme

The third experiment is to check if the proposed scheme works on non-equispaced grids as well. To this end, the CH is solved on the spatial interval $[0, 200]$ with the grid shown in Figure 5 ($N = 200$), and with the triangle shaped initial data

$$u(x,0) = \begin{cases} x - x_c + 20 & \text{if } x \in [x_c - 20, x_c), \\ -(x - x_c) + 20 & \text{if } x \in [x_c, 20), \\ 0 & \text{otherwise,} \end{cases}$$

where $x_c = 80.5$.

Figure 6 shows the numerical results by the three schemes, where the time mesh width is set to $\Delta t = 0.05$. For comparison, a result by a standard numerical method on finer equispaced mesh ($N = 2000$), marked as "FD/RK"

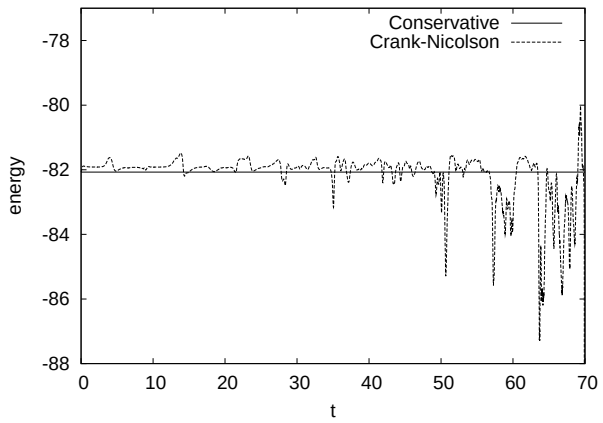

Figure 4: Evolution of the energies in the long-time computation

Figure 5: The non-uniform mesh ($N = 200$)

in the figures, is also presented. The scheme is obtained by discretizing space variable by the standard central finite-differences (with second-order accuracy), and then by discretizing time stepping by the standard 4th-order Runge–Kutta method. The time-stepping width is chosen considerably small ($\Delta t = 0.0005$) such that the result is accurate enough as a substitute for the unknown exact solution. As the solution suggests (Figure 6, bottom-right), in this problem setting the initial triangle shaped data soon splits into a number of peakons. The splitting mainly occurs at the center of the interval, which is the reason why the grid is chosen to be dense at the center. The result by the implicit Euler scheme (top-right) again exhibits strong dissipation, which can be also observed in the energy profile (Figure 7). The result by the proposed conservative scheme (Figure 6, top-left) is similar to the accurate result by FD/RK, with the excellent energy conservation profile (Figure 7). Compared to this result, even with considerably fine mesh sizes, the energy in FD/RK scheme monotonically moves apart from the exact value; this means that however mesh is refined the FD/RK method is not so reliable that it can be used as an integrator for long-time computations. The shape of the peakons in Crank–Nicolson case seems to be quite similar to the conservative and FD/RK cases (Figure 6, bottom-left). The energy profile, however, behaves dreadfully, where the error exceeds 10% in magnitude. In

this example, the peakons are quite sharp and high, and the slight error in the shapes of peakons is magnified as the big error in the energy.

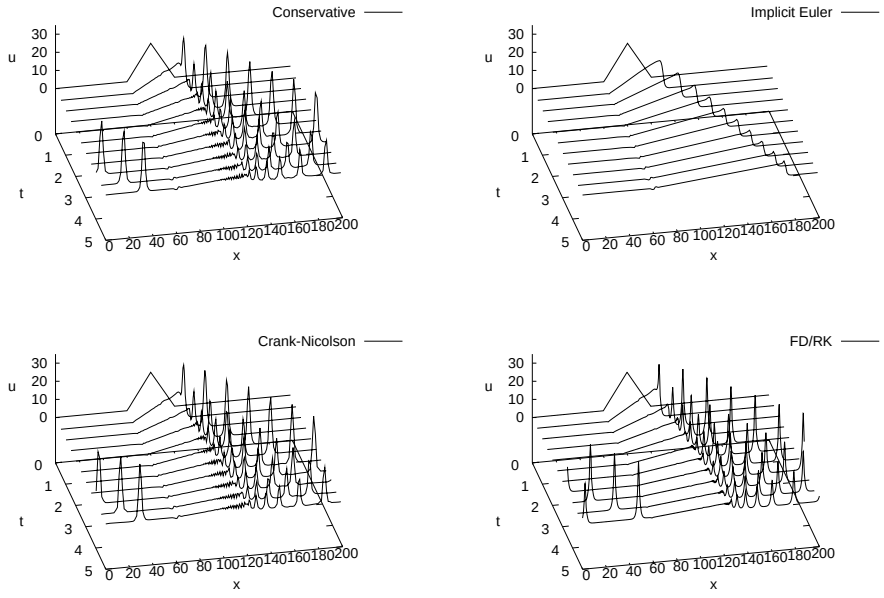

Figure 6: Generation of peakons; (top-left) the conservative scheme, (top-right) the implicit Euler scheme, (bottom-left) the Crank–Nicolson scheme, (bottom-right) the FD/RK solution on the finer mesh

4.3 The Dai equation

Scheme 3.1 is tested in the case of the Dai equation (3), which is an example of (1) with $\kappa = 0,\ \gamma \in \mathbb{R}$. This is quite similar to the limiting CH case, but now we have a freedom in the choice of γ. As described before, soliton solutions are expected to be smooth when $\gamma < 1$ and become "cusped" when $\gamma > 1$. Below we have tested two cases: $\gamma = 0.5$ and $\gamma = 1.4$. The energy function is

$$G(u, u_x) = -\frac{u^3 + \gamma u {u_x}^2}{2}, \tag{40}$$

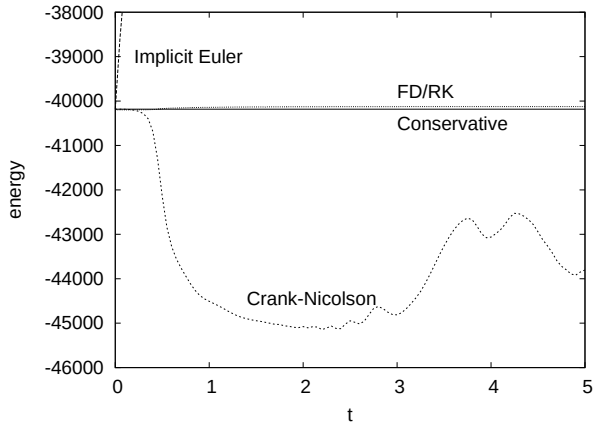

Figure 7: Evolution of the energies (peakon train case)

and accordingly the discrete partial derivatives are

$$\frac{\partial G_{\mathrm{d}}}{\partial (u^{(m+1)}, u^{(m)})} = -\frac{(u^{(m+1)})^2 + u^{(m+1)}u^{(m)} + (u^{(m)})^2}{2} - \gamma \left(\frac{(u_x^{(m+1)})^2 + (u_x^{(m)})^2}{4} \right), \tag{41}$$

$$\frac{\partial G_{\mathrm{d}}}{\partial (u_x^{(m+1)}, u_x^{(m)})} = -\gamma \left(\frac{u^{(m+1)} + u^{(m)}}{2} \right) \left(\frac{u_x^{(m+1)} + u_x^{(m)}}{2} \right). \tag{42}$$

We test Scheme 3.1 and the Crank–Nicolson scheme. The latter is constructed in a similar manner as in the previous section.

First, the case of $\gamma = 0.5$ is considered. With this parameter, solitons are smooth and the computation is rather easy. In order to check the long-time stability of the schemes, the problem is solved in a long interval $0 \le t \le 500$ with the temporal mesh size $\Delta t = 0.1$. The initial data is $u(x,0) = 5\,\mathrm{sech}(x-5) + 2\,\mathrm{sech}(x-15)$. The length of the spatial interval L is set to 40, for which the equispaced grid with $N = 200$ is employed (i.e. $\Delta x = 0.2$). Figure 8 shows the evolution of the numerical solutions. The computation proceeds quite stably as expected, and the shapes of the solitons are successfully preserved in both schemes, although the phase speeds of the solitons are different. Figure 9 shows the evolution of the energies. In the conservative scheme, the energy is strictly kept. In the Crank–Nicolson scheme, the energy oscillates, but stays near the exact value.

Next, the results with $\gamma = 1.4$ are presented. The equispaced grid on the spatial interval $[0, 40]$ with $N = 200$ or 400 is used, and the problem is

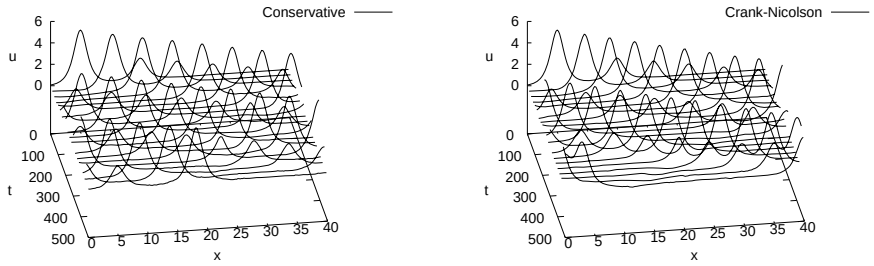

Figure 8: Smooth solitons in the Dai equation ($\gamma = 0.5$); (left) the conservative scheme, (right) the Crank–Nicolson scheme

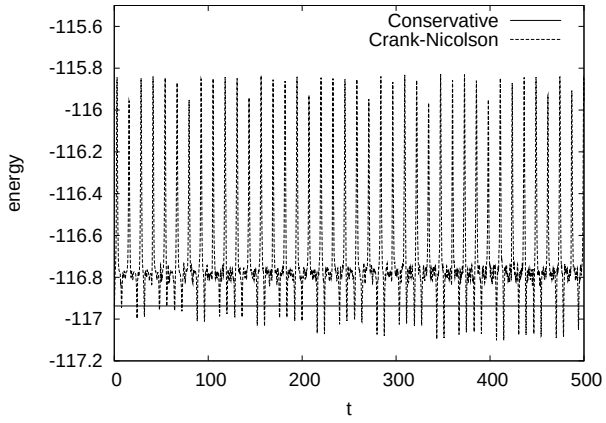

Figure 9: Evolution of the energies (the Dai equation, $\gamma = 0.5$)

solved in $0 \leq t \leq 10$ with the time mesh size $\Delta t = 0.1$. The initial data is set to the same one as in the limiting CH case, i.e., $u(x,0) = 5e^{-|x-x_a|} + 2e^{-|x-x_b|}$ with $x_a = (200/3 + 1/2)\Delta x$ and $x_b = (400/3 + 1/2)\Delta x$. Figure 10 shows the numerical solutions of $N = 400$, and Figure 11 the evolution of the energies in both $N = 200$ and 400 cases. From Figure 10, both schemes succeed in catching the peaked solutions (although numerically it is difficult to judge if the solutions are really "cusped" rather than "peaked"). Comparing Figure 11 (left) and Figure 9, we notice that with the same mesh ($N = 200$) the energy deviation in the Crank–Nicolson scheme becomes much larger when the solutions become singular, although it can be improved by refining the spatial mesh (Figure 11, right). In any case, the conservative scheme seems to be safer when we deal such singular solutions.

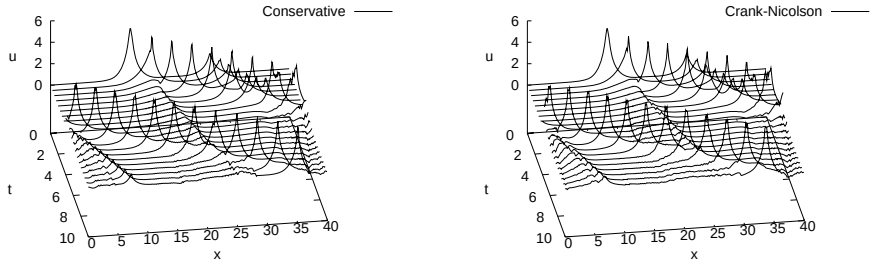

Figure 10: Cusped solutions in the Dai equation ($\gamma = 1.4, N = 400$); (left) the conservative scheme, (right) the Crank–Nicolson scheme

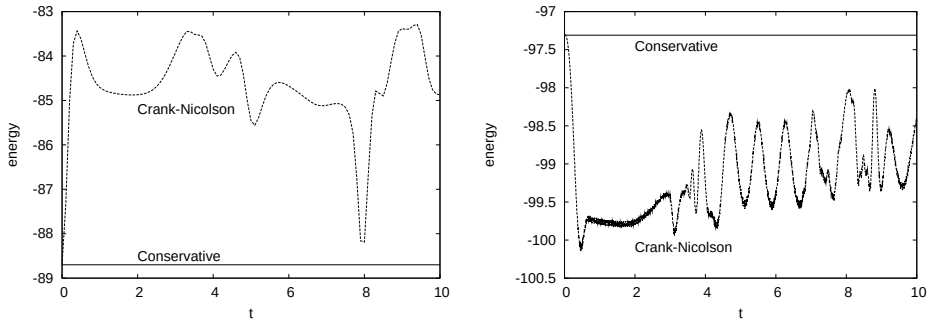

Figure 11: Evolution of the energies (the Dai equation, $\gamma = 1.4$); (left) $N = 200$, (right) $N = 400$

4.4 The BBM equation

In this section Scheme 3.1 is tested in the case of the BBM equation (4). The energy function is

$$G(u, u_x) = -\frac{u^3 + u^2}{2}, \tag{43}$$

and accordingly the discrete partial derivatives are

$$\begin{aligned} \frac{\partial G_{\mathrm{d}}}{\partial(u^{(m+1)}, u^{(m)})} &= -\frac{(u^{(m+1)})^2 + u^{(m+1)}u^{(m)} + (u^{(m)})^2}{2} \\ &\quad - \frac{u^{(m+1)} + u^{(m)}}{2}, \end{aligned} \tag{44}$$

$$\frac{\partial G_{\mathrm{d}}}{\partial(u_x^{(m+1)}, u_x^{(m)})} = 0. \tag{45}$$

The equation is considered over the spatial domain $[0, 40]$ using the equispaced mesh with the number of grid points $N = 100$. Then the problem is integrated in $0 \le t \le 20$ with the time mesh size $\Delta t = 0.25$. The initial data is set to $u(x, 0) = c_1 \mathrm{sech}(0.35(x - 15)) + c_2 \mathrm{sech}(0.25(x - 25))$, where $c_1 = 0.7^2/(1 - 0.7^2), c_2 = 0.5^2/(1 - 0.5^2)$ (see [16] for this initial data). The conservative scheme and the Crank–Nicolson scheme are tested. Figure 12 shows the numerical solutions, and Figure 13 the evolution of the energies. Both schemes successfully capture the propagation of the two-soliton. The conservative scheme strictly preserves the energy, while in the Crank–Nicolson scheme the energy oscillates around the exact value.

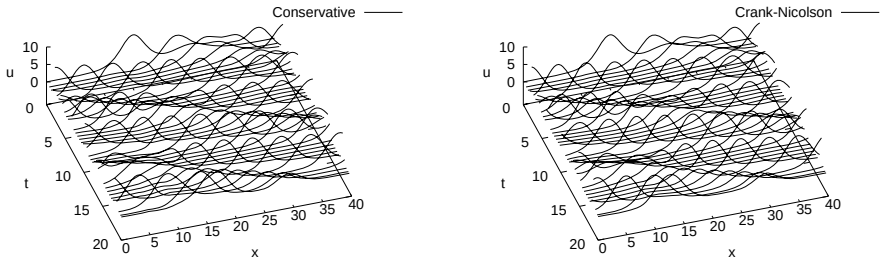

Figure 12: Two-soliton in the BBM equation; (left) the conservative scheme, (right) the Crank–Nicolson scheme

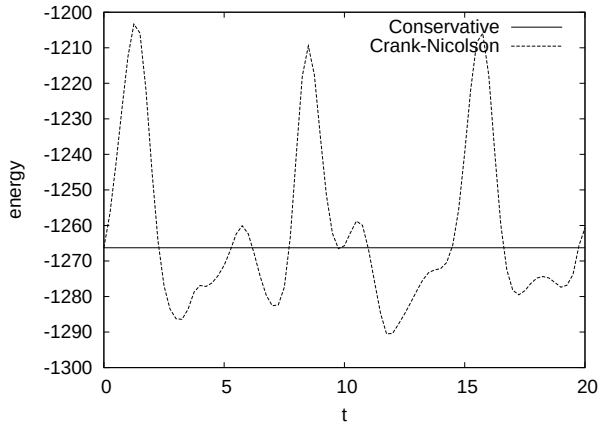

Figure 13: Evolution of the energies (the BBM equation)

5 Concluding remarks

In this paper a conservative Galerkin scheme for a class of nonlinear dispersive PDEs such as the Camassa–Holm equation has been proposed. The effectiveness of the scheme has been confirmed by numerical experiments.

Finally we would like to emphasize that the proposed scheme has an additional welcome feature that the conservation property would not be lost even if time mesh size is changed during the time evolution process. This can be easily understood by observing the facts that the scheme is a one-step method and that Theorem 3.2 holds for any Δt (as far as the scheme has a solution). This allows us to incorporate some adaptive time-stepping technique in the scheme in order to decrease computational cost, or to utilize the so-called composition technique (see, for example, [3]) in order to increase the temporal accuracy. This point should be another advantage of the proposed scheme over other standard numerical schemes, such as the Crank–Nicolson scheme employed in this paper. In the numerical experiments, the Crank–Nicolson scheme also showed good performance (if not the same level as the proposed scheme), but this might be caused by the time-symmetry of the scheme; it is generally known that, for time-symmetric differential equations, time-symmetric schemes quite often show far better behaviors than expected. However, as soon as some non-uniform time-stepping is introduced, the time-symmetry is destroyed, and accordingly the good performance would be lost. In fact, we did some experiments and found that the near-conservation of the energy (see, for example, Figure 9) dissolved under such circumstances.

Acknowledgments

Part of this work is supported by a Grant-in-Aid of the Ministry of Education, Culture, Sports, Science and Technology of Japan.

References

[1] Artebrant, R. and Schroll, H. J., Numerical Simulation of Camassa–Holm Peakons by Adaptive Upwinding, *Appl. Numer. Math.*, **56** (2006), 695–711.

[2] Benjamin, T. B., Bona, J. L. and Mahony, J. J., Model Equations for Long Waves in Nonlinear Dispersive Systems, *Phil. Trans. Roy. Soc. (London)*, **272** (1972), 47–78.

[3] Budd, C. J. and Piggott, M. D., Geometric Integration and Its Applications, *Handbook of numerical analysis*, **XI**, North-Holland, Amsterdam, 2003, 35–139.

[4] Brezis, H., Analyse Fonctionnelle, Masson, Paris, 1983.

[5] Camassa, R. and Holm, D. D., An Integrable Shallow Water Equation with Peaked Solitons, *Phys. Rev. Lett.*, **71** (1993), 1661–1664.

[6] Camassa, R., Holm, D. D. and Hyman, J. M., A New Integrable Shallow Water Equation, *Adv. Appl. Mech.*, **31** (1994), 1–33.

[7] Coclite, G. M., Holden, H. and Karlsen, K. H., Global Weak Solutions to a Generalized Hyperelastic-Rod Wave Equation, *SIAM J. Math. Anal.*, **37** (2005), 1044-1069.

[8] Cohen, D., Owren, B. and Raynaud, X., Multi-symplecetic integration of the Camassa–Holm equation, submitted.

[9] Constantin, A. and Escher, J., Global Existence and Blow-up for a Shallow Water Equation, *Ann. Scuola Norm. Sup. Pisa Cl. Sci.*, **XXVI** (1998), 303–328.

[10] Constantin, A. and Molinet, L., Global Weak Solutions for a Shallow Water Equation, *Comm. Math. Phys.*, **211** (2000), 45–61.

[11] Constantin, A. and Strauss, W. A., Stability of a Class of Solitary Waves in Compressible Elastic Rods, *Phys. Lett. A*, **270** (2000), 140–148.

[12] Constantin, A. and Strauss, W. A., Stability of Peakons, *Comm. Pure Appl. Math.*, **LIII** (2000), 603–610.

[13] Dai, H. H., Model Equations for Nonlinear Disperwive Waves in a Compressible Mooney-Rivlin Rod, *Acta Mech.*, **127** (1998).

[14] Dai, H. H. and Huo, Y., Solitary Shock Waves and Other Travelling Waves in a General Compressible Hyperelastic Rod, *Proc. R. Soc. Lond. A*, **456** (2000), 331–363.

[15] Eilbeck, J. C. and McGuire, G. R., Numerical Study of the Regularized Long-Wave Equation I: Numerical Methods, *J. Comput. Phys.*, **19** (1975), 43–57.

[16] Eilbeck, J. C. and McGuire, G. R., Numerical Study of the Regularized Long-Wave Equation II: Interaction of Solitary Waves, *J. Comput. Phys.*, **23** (1977), 63–73.

[17] Fuchssteiner, B. and Fokas, A. S., Symplectic Structures, Their Bäcklund Transformations and Hereditary Symmetries, *Phys. D*, **4** (1981), 47–66.

[18] Furihata, D., Finite Difference Schemes for $\frac{\partial u}{\partial t} = \left(\frac{\partial}{\partial x}\right)^{\alpha} \frac{\delta G}{\delta u}$ That Inherit Energy Conservation or Dissipation Property, *J. Comput. Phys.*, **156** (1999), 181–205.

[19] Guo, L. and Chen, H., H^1-Galerkin Mixed Finite Element Method for the Regularized Long Wave Equation, *Computing*, **77** (2006), 205–221.

[20] Holden, H. and Raynaud, X., A Convergent Numerical Scheme for the Camassa–Holm Equation Based on Multipeakons *Disc. Cont. Dyn. Sys.*, **14** (2006), 505–523.

[21] Holden, H. and Raynaud, X., Convergence of a Finite Difference Scheme for the Camassa–Holm Equation, *SIAM J. Numer. Anal.*, **44** (2006), 1655–1680.

[22] Kalische, H. and Lenells, J., Numerical Study of Traveling-Wave Solutions for the Camassa–Holm Equation, *Chaos, Sol. Frac.*, **25** (2005), 287–298.

[23] Leimkuhler, B. and Reich, S., Simulating Hamiltonian Dynamics, Cambridge University Press, Cambridge, 2004.

[24] Matsuo, T., Dissipative/conservative Galerkin Method using Discrete Partial Derivatives for Nonlinear Evolution Equations, to appear in *J. Comput. Appl. Math.* (available online with doi:10.1016/j.cam.2007.08.001).

[25] Matsuo, T. and Furihata, D., Dissipative or Conservative Finite Difference Schemes for Complex-Valued Nonlinear Partial Differential Equations, *J. Comput. Phys.*, **171** (2001), 425–447.

[26] Takeya, K. and Furihata, D., private communication.

[27] Whitham, G. B., Linear and Nonlinear Waves, John Wiley & Sons, New York, 1974.

[28] Yin, Z., On the Blow-Up of Solutions of a Periodic Nonlinear Dispersive Wave Equation in Compressible Elastic Rods, *J. Math. Anal. Appl.*, **288** (2003), 232–245.